Penerbit Akademia Baru

CFD Letters

Journal homepage: www.akademiabaru.com/cfdl.html
ISSN: 2180-1363

Significances of Homogeneous-Heterogeneous Reactions on Casson Fluid over a Slippery Stretchable Rotating Disk with Variable Thickness

Open Access

Hanumesh Vaidya[1], Kerehalli Vinayaka Prasad[2,*], Srikantha Setty B[2]

[1] Department of Mathematics, SSA Government First Grade College (Autonomous), Ballari-583 101, Karnataka, India
[2] Department of Mathematics, VSK University, Vinayaka Nagar, Ballari-583 105, Karnataka, India

ARTICLE INFO

Article history:
Received 4 January 2019
Received in revised form 16 March 2019
Accepted 20 April 2019
Available online 26 April 2019

ABSTRACT

In the present paper, the effect of homogeneous-heterogeneous reactions on MHD Casson fluid over a stretchable rotating disk with variable thickness is examined. Slip effects are taken into account. The governing coupled nonlinear partial differential equations are reduced into a system of coupled nonlinear ordinary differential equations by using Von Karman similarity transformation. Further, solutions are obtained via efficient semi-analytical method Optimal Homotopy Analysis Method (OHAM). The results are presented graphically in order to see the influence of pertinent parameters on the velocity and concentration fields. Homogeneous reaction parameter and heterogeneous reaction parameter have a converse impact on fluid concentration.

Keywords:
Rotating disk, Homogeneous – heterogeneous reaction, variable thickness, Optimal Homotopy Analysis Method

1. Introduction

In recent years, numerous researchers have attracted towards the fluid flow by a rotating disk. It is because of its remarkable applications in engineering and industrial areas such as jet motors, computer storage devices, rotating machinery, medical equipment, spin coating and many others. The pioneering work of Von Karman [1] on hydrodynamic flow over an infinite rotating disk has given a new dimension to fluid flow over a rotating disk. He also presented the well-known transformation which reduces the governing partial differential equations into ordinary differential equations. Cochran's [2] analyzed the rotating disk problem which was considered by Von Karman [1] and obtained a higher degree of accuracy via asymptotic solutions. Further, Batchelor [3] examined the work of Ref [1] and contended that the fundamental assemblage of liquid would spool with steady angular velocity and boundary layers would create on both the discs as the Reynolds number expanded. Stewartson [4] demonstrated experimentally and theoretically that the rotation of the

*Corresponding author.
E-mail address: prasadkv2007@gmail.com (K.V. Prasad)

main body of fluid depends on the rotation of the disc and in continuation to this, Benton [5] improved Cochran's method of solutions by considering the unsteady case. The concept of fluid flow over a rotating disk was revisited by Anderson *et al.,* [6] and Ming [7] with the analysis of the non-Newtonian fluid. Ahmad [8] studied the impact of variable liquid properties flow due to a porous rotating disk. Further, Yin *et al.,* [9] examined the flow and heat transfer conduct of nanofluid due to a rotating disk. Sheikholeslami *et al.,* [10] studied the impact of centrifugal and gravitational forces on nanofluid spraying on an inclined rotating disk. Yin *et al.,* [11] extended the work of Ref [9] by considering three types of nanoparticles-Cu, Al_2O_3 and CuO-with water-based nanofluids.

The surface of sheet/disc can be considered with variable thickness because it's many industrial applications such as in architectural, mechanical, civil, aeronautical and marine engineering. Fang *et al.,* [12] explored the liquid flow over a variable thickened surface. Xun *et al.,* [13] extended the work of Fang *et al.,* [12] to the rotating disk and scrutinized the MHD flow of Ostwalde- wale fluid with decreasing power-law index parameter. Hayat *et al.,* [14] examined the flow due to a rotating disk with a thickness in the presence of radiation. Imtiaz *et al.,* [15] considered the slip velocity at the solid-fluid interface and studied the characteristics of magnetohydrodynamic flow by a rotating variable thickened disk. Moreover, Prasad *et al.,* [16-20] examined analytically the geometry of the variable thickened surface with nanofluid/ Casson nanofluid with different external effects.

Homogeneous and heterogeneous reactions occur in a wide variety of chemically reacting systems namely, combustion, catalysis and biochemical systems. These reactions generally take place in food processing, manufacturing of ceramics, the formation of fog, production of polymers, crops damaging due to freezing, electric power generating systems and many others. Choudary and Merkin [21] who initiated the work on a simple isothermal model for homogeneous and heterogeneous reactions in boundary layer flow with similar diffusivities. Chowdary and Merkin [22] revisited and extended their previous work by taking two different diffusivities. They have taken homogeneous reactions by cubic autocatalysis and heterogeneous reaction by the first-order isothermal process. Merkin [23] studied the isothermal model for homogeneous and heterogeneous reactions for flow over a flat plate. The influence on the stagnation point flow towards the stretching sheet with chemical reactions was examined by Bachok and Ishak [24]. Kameshwaran *et al.,* [25] examined the effects of homogeneous and heterogeneous reactions in a nanofluid flow over a porous stretching/shrinking sheet. Impact of melting heat transfer and homogeneous-heterogeneous reactions on MHD flow has been reported by Hayat *et al.,* [26]. Effect of homogeneous and heterogeneous reactions on the Ferrofluids over a rotating disk was analyzed by Hayat *et al.,* [27] by taking the viscous dissipation into account. Lavanya [28] studied the MHD rotating flow over a porous channel in presence of magnetic field. An experimental analysis of the thermal effect on viscoelastic elastomer by considering magnetic effect was reported by Touraband Aguib [29] and several researchers have examined the Newtonian fluid/non-Newtonian fluid considering heat transfer with different geometries and configurations [30-36].

To the best of the author's knowledge, no attempt has been made to study the Casson fluid over a stretchable rotating variable thickened disk. The present paper aims to investigate the effects of slip velocity and homogeneous-heterogeneous on a Casson fluid over a stretchable rotating variable thickened disk. The coupled governing nonlinear partial differential equations are converted into a system of coupled nonlinear ordinary differential equations by using Von Karman similarity transformation. The transformed equations are solved semi analytically via Optimal Homotopy Analysis Method (OHAM) (See [37-38]). Convergence analysis and error analyses of obtained solutions are confirmed overtly. Various physical parameters on velocity and concentration fields are evaluated and plotted graphically. Skin friction is deliberated through different flow variables. With certain limiting conditions the present investigation is compared with published literature.

2. Methodology
2.1 Mathematical Formulation

Let us consider two dimensional steady, viscous, incompressible and axisymmetric flow of an electrically conducting non-Newtonian fluid model namely, Casson fluid model over a stretchable rotating disk with the homogeneous and heterogeneous chemical reactions. A simple model for a homogeneous and heterogeneous chemical reaction is given by,

$$A + 2B \rightarrow 3B, \text{ rate } = k_1 a b^2 \tag{1}$$

The single, first order isothermal chemical reaction on the catalyst surface is

$$A \rightarrow B, \text{ rate } = k_2 a \tag{2}$$

where a and b are the dimensionless concentration of the chemical species A and B, k_1 and k_2 are rate constants. We consider both the reaction processes are isothermal. Further, the fluid occupies the semi-infinite region over a stretchable rotating disk placed at a variable thickness $z = c\left(r/R_0 + 1\right)^{-m}$ and disk rotates with an angular velocity Ω and the stretching rate c_1. Here c is the disk thickness coefficient, m is the disk thickness index and R_0 is the feature radius of the disk. The rheological equation of state for anisotropic and incompressible Casson fluid is given by,

$$\tau_{ij} = \begin{cases} 2\left(\mu_B + P_y / \sqrt{2\pi}\right) e_{ij,} & \pi > \pi_c \\ 2\left(\mu_B + P_y / \sqrt{2\pi_c}\right) e_{ij,} & \pi < \pi_c \end{cases} \tag{3}$$

where $\pi = e_{ij} e_{ij}$ and e_{ij} is the $(i, j)^{\text{th}}$ component of deformation rate, π is the product of component with itself, π_c is a critical value of this product based on the non-Newtonian model, μ_B is the plastic dynamic viscosity of the non-Newtonian fluid and P_y is the yield stress of the fluid. The physical model of the variable thickened rotating disk is as shown in Figure 1.

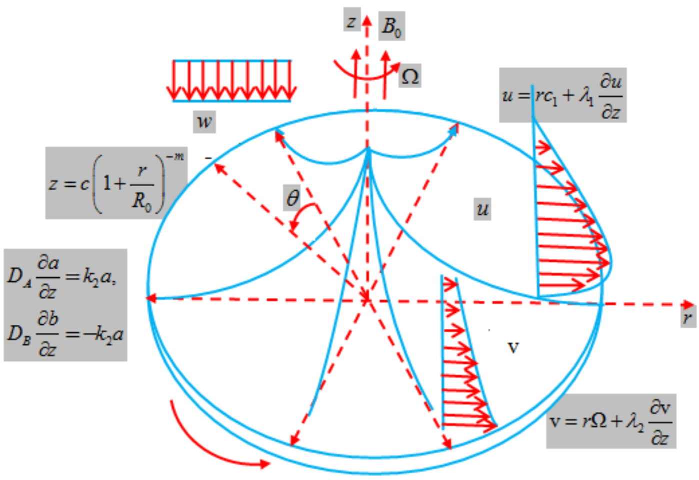

Fig. 1. Physical model of the rotating disk

Thereafter, it is assumed that a uniform magnetic strength B_0 is employed perpendicular to the circular disk along the z-axis. The effect of the induced magnetic field is to be ignored under the hypothesis of a small magnetic Reynolds number. Under these assumptions and usual boundary layer approximations, the governing equations for the continuity, the momentum and the concentration in cylindrical polar coordinates are,

$$\frac{\partial u}{\partial r}+\frac{u}{r}+\frac{\partial w}{\partial z}=0 \tag{4}$$

$$\rho\left(u\frac{\partial u}{\partial r}+w\frac{\partial u}{\partial z}-\frac{\mathrm{v}^2}{r}\right)=\mu\left(1+\frac{1}{\beta}\right)\frac{\partial^2 u}{\partial z^2}-\sigma B_0^2 u \tag{5}$$

$$\rho\left(u\frac{\partial \mathrm{v}}{\partial r}+w\frac{\partial \mathrm{v}}{\partial z}+\frac{u\mathrm{v}}{r}\right)=\mu\left(1+\frac{1}{\beta}\right)\frac{\partial^2 \mathrm{v}}{\partial z^2}-\sigma B_0^2 \mathrm{v} \tag{6}$$

$$u\frac{\partial a}{\partial r}+w\frac{\partial a}{\partial z}=D_A\frac{\partial^2 a}{\partial z^2}-k_1ab^2 \tag{7}$$

$$u\frac{\partial b}{\partial r}+w\frac{\partial b}{\partial z}=D_B\frac{\partial^2 b}{\partial z^2}+k_1ab^2 \tag{8}$$

The appropriate boundary conditions for the problem is given by,

$$\begin{aligned}&u=rc_1+\lambda_1\frac{\partial u}{\partial z},\ \mathrm{v}=r\Omega+\lambda_2\frac{\partial \mathrm{v}}{\partial z},\quad w=0,\ D_A\frac{\partial a}{\partial z}=k_2a,\quad D_B\frac{\partial b}{\partial z}=-k_2a\quad \text{at}\quad z=c\left(1+r/R_0\right)^{-m}\\ &u\to 0,\quad \mathrm{v}\to 0,\quad a\to a_0,\quad b\to 0\quad as\ z\to\infty\end{aligned} \tag{9}$$

where u, v and w are the velocity components in the direction of r,θ and z respectively. ρ is the density of the fluid, μ is the viscosity of the fluid, σ is the electrical conductivity, β is the Casson parameter, B_0 is the magnetic flux density, D_A and D_B are the diffusion species coefficients of A and B, λ_1 and λ_2 are the velocity slip coefficients along u and v directions respectively.

Von-Karman similarity transformations are

$$\begin{aligned}&u=r\Omega F(\eta),\ \mathrm{v}=r\Omega G(\eta), w=R_0\Omega\left(1+r/R_0\right)^{-m}\left(\Omega R_0^2/v\right)^{-1/n+1}H(\eta),\\ &a=a_0\phi(\eta), b=a_0J(\eta),\quad \eta=\frac{z}{R_0}\left(1+r/R_0\right)^{m}\left(\Omega R_0^2/v\right)^{1/n+1}\end{aligned} \tag{10}$$

Using Eq. (10) in to Eq. (4-8) reduces to the following system of coupled highly nonlinear ordinary differential equations.

$$H'+2F+m\varepsilon\eta F'=0 \tag{11}$$

$$\mathrm{Re}^{(1-n/1+n)}\left(1+R\right)^{2m}\left(1+\frac{1}{\beta}\right)F''-F^{2}-m\varepsilon\eta FF'+G^{2}-HF'-Mn\,F=0 \tag{12}$$

$$\mathrm{Re}^{(1-n/1+n)}\left(1+R\right)^{2m}\left(1+\frac{1}{\beta}\right)G''-2FG-HG'-m\varepsilon\eta FG'-Mn\,G=0 \tag{13}$$

$$\frac{1}{Sc}\mathrm{Re}^{(1-n/1+n)}\left(1+R\right)^{2m}\phi''-m\varepsilon\eta F\phi'-H\phi'-K\phi J^{2}=0 \tag{14}$$

$$\frac{\delta}{Sc}\mathrm{Re}^{(1-n/1+n)}\left(1+R\right)^{2m}J''-m\varepsilon\eta FJ'-HJ'+K\phi J^{2}=0 \tag{15}$$

Subjected to the boundary conditions,

$$\begin{aligned}
&H(\alpha)=0, && F(\alpha)=A_{1}+\gamma_{1}(1+R)^{m}F'(\alpha),\\
&G(\alpha)=1+\gamma_{2}(1+R)^{m}G'(\alpha), && \phi'(\alpha)=k_{s}\phi(\alpha),\ \delta J'(\alpha)=-k_{s}J(\alpha),\\
&F(\infty)\to 0,\quad G(\infty)\to 0, && \phi(\infty)\to 1,\quad J(\infty)\to 0
\end{aligned} \tag{16}$$

where $\varepsilon=r/\left(r+R_{0}\right)$ is a dimensionless constant, $\mathrm{Re}=\left(\Omega R_{0}^{2}/v\right)$ is a Reynolds number, $R=r/R_{0}$ is the dimensionless radius, $\alpha=\left(c/R_{0}\right)\left(\Omega R_{0}^{2}/v\right)^{-1/n+1}$ is the dimensionless disk thickness coefficient, $Mn=\left(\sigma B_{0}^{2}/\rho\Omega\right)$ is the Hartmann number, $Sc=\left(v/D_{A}\right)$ is the Schmidt number, $K=\left(k_{1}a_{0}^{2}/\Omega\right)$ is the measure of strength of homogeneous reaction, $A_{1}=\left(c_{1}/\Omega\right)$ is scaled stretching parameter, $\gamma_{1}=\left(\lambda_{1}/R_{0}\right)\left(\Omega R_{0}^{2}/v\right)^{1/n+1}$, $\gamma_{2}=\left(\lambda_{2}/R_{0}\right)\left(\Omega R_{0}^{2}/v\right)^{1/n+1}$ are velocity slip parameters, $k_{s}=\left(k_{2}R_{0}/D_{A}\right)\left(1+r/R_{0}\right)^{-m}\left(\Omega R_{0}^{2}/v\right)^{-1/n+1}$ is the measure of strength of the heterogeneous reaction, $\delta=\left(D_{B}/D_{A}\right)$ is the ratio of the diffusion coefficient. In most instances, it can be assumed that the diffusion coefficients of chemical species A and B are of similar size. This postulate provides us to make the assumption that the diffusion coefficients D_{A} and D_{B} are equal $\left(i.e.\,\delta=1\right)$, then we have,

$$\phi(\eta)+J(\eta)=1 \tag{17}$$

using Eq. (17), Eq. (14) and Eq. (15) reduces to,

$$\frac{1}{Sc}\mathrm{Re}^{(1-n/1+n)}\left(1+R\right)^{2m}\phi''-m\varepsilon\eta F\phi'-H\phi'-K\phi\left(1-\phi\right)^{2}=0 \tag{18}$$

Corresponding boundary conditions become,

$$\phi'(\alpha)=k_{s}\phi(\alpha),\ \phi(\infty)\to 1 \tag{19}$$

For the computation purpose, we define,

$$H(\eta)=h(\xi), F(\eta)=f(\xi), G(\eta)=g(\xi),\ \phi(\eta)=\phi(\xi)\ \text{where}\ \xi=(\eta-\alpha) \tag{20}$$

by using Eq. (20) in similarity Eq. (11-13) and Eq. (18) becomes

$$h'+2f+m\varepsilon(\alpha+\xi)f'=0 \tag{21}$$

$$\mathrm{Re}^{(1-n/1+n)}(1+R)^{2m}\left(1+\frac{1}{\beta}\right)f''-f^2-m\varepsilon(\alpha+\xi)ff'+g^2-hf'-Mn\,f=0 \tag{22}$$

$$\mathrm{Re}^{(1-n/1+n)}(1+R)^{2m}\left(1+\frac{1}{\beta}\right)g''-2fg-hg'-m\varepsilon(\alpha+\xi)fg'-Mn\,g=0 \tag{23}$$

$$\frac{1}{Sc}\mathrm{Re}^{(1-n/1+n)}(1+R)^{2m}\phi''-m\varepsilon(\alpha+\xi)f\phi'-h\phi'-K\phi(1-\phi)^2=0 \tag{24}$$

with corresponding boundary conditions are,

$$\begin{aligned} &h(0)=0, && f(0)=A_1+\gamma_1(1+R)^m f'(0),\\ &g(0)=1+\gamma_2(1+R)^m g'(0), && \phi'(0)=k_s\phi(0),\\ &f(\infty)\to 0,\quad g(\infty)\to 0, && \phi(\infty)\to 1 \end{aligned} \tag{25}$$

Here prime denotes derivative with respect to ξ and h, f, g and ϕ are axial, radial, tangential velocity profiles and concentration profile respectively.

The important physical quantity of engineering interest in this problem is the skin friction coefficient C_f which is given by,

$$C_f=\left(1+\frac{1}{\beta}\right)\left(\frac{\sqrt{\left((\tau_{zr})^2+(\tau_{z\theta})^2\right)}}{\rho(r\Omega)^2}\right) \tag{26}$$

where τ_{zr} *and* $\tau_{z\theta}$ are called radial and tangential shear stress at the surface of the disk and is defined by,

$$\tau_{zr}=\mu\left(\frac{\partial u}{\partial z}\right)_{at\ z=A_1(1+R)^{-m}},\quad \tau_{z\theta}=\mu\left(\frac{\partial v}{\partial z}\right)_{at\ z=A_1(1+R)^{-m}}$$

Substitute Eq. (10) in Eq. (26) we get,

$$C_f(\mathrm{Re})^{\left(\frac{n}{1+n}\right)}=\left(1+\frac{1}{\beta}\right)\frac{(1+R)^m}{R}\left[\left(f'(0)\right)^2+\left(g'(0)\right)^2\right]^{1/2} \tag{27}$$

2.2 Method of Solution
2.2.1 Optimal Homotopy Analysis Method (OHAM)

Optimal Homotopy analysis method has been applied to solve nonlinear coupled ordinary differential Eq. (21) to Eq. (24) with corresponding boundary conditions Eq. (25). The OHAM scheme breaks down a nonlinear differential equation into an infinite number of linear subproblems whose solutions are found analytically. In the frame of OHAM, we are independent to pick the auxiliary linear operator and introductory approximation. This is worthwhile over the other iterative procedures where convergence is to a great extent attached to a decent initial approximation of the solution. The OHAM differs from other analytical approximation methods as it does not depend on small or large physical parameters. This is obtained by employing artificial convergence control parameters which guaranty convergence of the series solution. The OHAM has been successfully applied to a wide range of nonlinear problems. Now we assume the initial guesses for axial, radial, tangential velocities and concentration according to the given boundary conditions Eq. (25),

$$h_0(\xi)=0,\;\; f_0(\xi)=\frac{A_1}{1+\gamma_1(1+R)^m}e^{-\xi},\; g_0(\xi)=\frac{1}{1+\gamma_2(1+R)^m}e^{-\xi},\; \phi_0(\xi)=1-\left(\frac{1}{2}\right)e^{-k_s\xi} \tag{28}$$

We select the linear operators in the form,

$$L_h=\frac{d}{d\xi},\;\; L_f=\frac{d^2}{d\xi^2}-f,\;\; L_g=\frac{d^2}{d\xi^2}-g,\;\; L_\phi=\frac{d^2}{d\xi^2}+k_s\frac{d}{d\xi} \tag{29}$$

The expressions of exact residual errors are written as:

$$\begin{aligned}
\bar{E}_p^h(\hbar_h)&=\int_0^1\left(N_h\left[\sum_{y=0}^{p}\hat{h}_y(\xi)\right]\right)^2 d\xi\\
\bar{E}_p^f(\hbar_f)&=\int_0^1\left(N_f\left[\sum_{y=0}^{p}\hat{f}_y(\xi)\right]\right)^2 d\xi\\
\bar{E}_p^g(\hbar_g)&=\int_0^1\left(N_g\left[\sum_{y=0}^{p}\hat{g}_y(\xi)\right]\right)^2 d\xi\\
\bar{E}_p^\phi(\hbar_\phi)&=\int_0^1\left(N_\phi\left[\sum_{y=0}^{p}\hat{\phi}_y(\xi)\right]\right)^2 d\xi
\end{aligned} \tag{30}$$

We used the average squared residual errors instead of exact residual errors $\bar{E}_p^h(\hbar_h)$, $\bar{E}_p^f(\hbar_f)$, $\bar{E}_p^g(\hbar_g)$ and $\bar{E}_p^\phi(\hbar_\phi)$ because they have taken much time.

$$
\begin{aligned}
\bar{E}_p^h(\hbar_h) &= \frac{1}{P+1}\sum_{y=0}^{P}\left(N_h\left[\hat{h}_{[P]}(\xi_y), \hat{f}_{[P]}(\xi_y)\right]\right)^2 \\
\bar{E}_p^f(\hbar_f) &= \frac{1}{P+1}\sum_{y=0}^{P}\left(N_f\left[\hat{f}_{[P]}(\xi_y), \hat{h}_{[P]}(\xi_y), \hat{g}_{[P]}(\xi_y)\right]\right)^2 \\
\bar{E}_p^g(\hbar_g) &= \frac{1}{P+1}\sum_{y=1}^{P}\left(N_g\left[\hat{g}_{[P]}(\xi_y), \hat{h}_{[P]}(\xi_y), \hat{f}_{[P]}(\xi_y)\right]\right)^2 \\
\bar{E}_p^\phi(\hbar_\phi) &= \frac{1}{P+1}\sum_{y=0}^{P}\left(N_\phi\left[\hat{\phi}_{[P]}(\xi_y), \hat{f}_{[P]}(\xi_y), \hat{h}_{[P]}(\xi_y)\right]\right)^2
\end{aligned} \tag{31}
$$

$$
\bar{E}_p^t(\hbar) = \bar{E}_p^h(\hbar_h) + \bar{E}_p^f(\hbar_f) + \bar{E}_p^g(\hbar_g) + \bar{E}_p^\phi(\hbar_\phi) \tag{32}
$$

where $\bar{E}_p^t(\hbar)$ is the total residual error, $\xi_y = y/P, y = 0,1,..P.$ Now we minimize the error function $\bar{E}_p^h(\hbar_h), \bar{E}_p^f(\hbar_f), \bar{E}_p^g(\hbar_g)$ and $\bar{E}_p^\phi(\hbar_\phi)$ in $\hbar_h, \hbar_f, \hbar_g, \hbar_\phi$ and obtain the optimal value of $\hbar_h, \hbar_f, \hbar_g, \hbar_\phi$. For pth order approximation, the optimal value of $\hbar_h, \hbar_f, \hbar_g, \hbar_\phi$ for h, f, g, ϕ is given by, $\frac{\partial \bar{E}_p^h(\hbar_h)}{\partial h} = 0, \frac{\partial \bar{E}_p^f(\hbar_f)}{\partial h} = 0, \frac{\partial \bar{E}_p^g(\hbar_g)}{\partial h} = 0, \frac{\partial \bar{E}_p^\phi(\hbar_\phi)}{\partial h} = 0$ respectively. Evidently, $\lim_{p\to\infty} \bar{E}_p^h(\hbar_h), \lim_{p\to\infty} \bar{E}_p^f(\hbar_f)$, $\lim_{p\to\infty} \bar{E}_p^g(\hbar_g), \lim_{p\to\infty} \bar{E}_p^\phi(\hbar_\phi)$ corresponding to a convergent series solution. Table 1 represents the values of the individual average squared residual error at a different order of approximations by considering the optimal values of $\hbar_h = -1.365, \hbar_f = -1.2209, \hbar_g = -1.23586, \hbar_\phi = -0.295229$ which have been obtained by minimizing the averaged residual errors at the 12th order approximation. It can be clearly observed that average squared residual errors are getting smaller and smaller as we increase the order of approximations. As such, by taking the order of approximation sufficiently large and by picking the convergence control parameters to minimize the average squared residual error, we can get accurate solutions.

Table 1
Individual average squared residual error as a function of the number of iterations when parameters are fixed at $\mathrm{Re} = 0.9, A_1 = 0.3, n = 0.5, m = 0.5, Mn = 1, \alpha = 1.2,$ $\gamma_1 = \varepsilon = 0.3, \gamma_2 = 0.4, \beta = 10, \ K = k_s = Sc = 0.5.$ We have optimal convergence control parameter values of $\hbar_h = -1.365, \hbar_f = -1.2209,$ $\hbar_g = -1.23586, \hbar_\phi = -0.295229.$

p	$\bar{E}_p^h$	$\bar{E}_p^f$	$\bar{E}_p^g$	$\bar{E}_p^\phi$	CPU time (s)
2	5.63×10^{-3}	2.74×10^{-3}	1.08×10^{-3}	2.67×10^{-6}	8.10522
4	3.67×10^{-4}	2.98×10^{-5}	3.11×10^{-4}	3.06×10^{-7}	53.5464
6	2.04×10^{-5}	7.34×10^{-6}	3.81×10^{-5}	2.19×10^{-7}	254.843
8	1.28×10^{-6}	1.24×10^{-6}	2.94×10^{-6}	4.03×10^{-8}	1093.12
10	1.59×10^{-7}	1.16×10^{-7}	5.87×10^{-7}	2.09×10^{-8}	4373.54
12	2.77×10^{-8}	2.86×10^{-8}	2.29×10^{-7}	1.23×10^{-8}	15389.4

2.2.2 Validation of methodology

Here, the exactness of the OHAM technique which is employed to solve the present problems is described. Without loss of all-inclusive statement, consider the case where $\mathrm{Re}=0.9, A_1=0.3, n=0.5, m=0.5, Mn=1, \alpha=1.2, \gamma_1=\varepsilon=0.3, \gamma_2=0.4, \beta=10, K=k_s=Sc=0.5$. The 12th- order approximate solution is recorded. The corresponding optimal convergence-control parameters are found to be $\hbar_h=-1.365, \hbar_f=-1.2209, \hbar_g=-1.23586, \hbar_\phi=-0.295229$. Moreover; it is found that the residual error of each governing equation diminishes as a function of the order of approximation, as appeared in Figure 2.

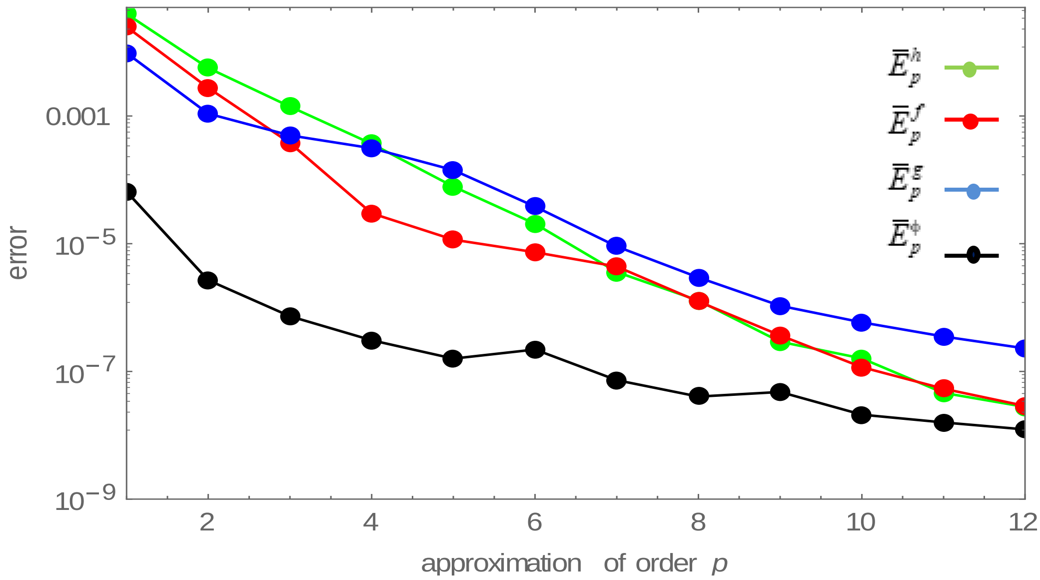

Fig. 2. Residual error vs. Order of approximation

For the validation of the OHAM, the results are compared with the available results in the literature (see Table 2) and the comparison shows an excellent agreement with the results of Anderson *et al.,* [6], Ming *et al.,* [7], Xun *et al.,* [13], and Hayat *et al.,* [14].

Table 2
Comparison of results for $f'(0)$ and $-g'(0)$ when
$m=A_1=Mn=\gamma_1=\gamma_2=0, \alpha=1.2,$
$Sc=K=ks=0.5, \varepsilon=0.5, n=1, \mathrm{Re}=0.9, \beta\to\infty.$

Skin friction	Anderson *et al.,* [6]	Ming *et al.,* [7]	Xun *et al.,* [13]	Hayat *et al.,* [14]	Present Result
$f'(0)$	0.510	0.51021	0.510231	0.5109	0.5115
$-g'(0)$	0.616	0.61591	0.615921	0.61598	0.61405

3. Results

The main objective of this section is to present the analysis of the graphical results obtained for various pertinent parameters namely, dimensionless constant ε, disk thickness coefficient α, disk thickness index m, velocity slip parameters λ_1 and λ_2, Hartmann number Mn, Casson fluid parameter β, power law exponent parameter n, Reynolds number Re, strength of heterogeneous reaction parameter k_s, Schmidt number Sc, strength of homogeneous reaction parameter K, scaled stretching parameter A1on axial velocity $h(\xi)$, radial velocity $f(\xi)$, tangential velocity $g(\xi)$ and concentration field $\phi(\xi)$. The numerical result of skin friction $(f'(0)\ and\ g'(0))$ for various physical parameters is tabulated in Table.3.

Figure 3(a) through 3(d) elucidates that the impact of α and m on velocity and concentration field. For $m<0$, all the three velocity fields decreases whereas the concentration field increases for higher the value of α and exactly the opposite trend is observed in the case of $m>0$. This is evident from the expression $\alpha=(c/R_0)(\Omega R_0^2/\nu)^{-1/n+1}$ that α is inversely proportional to feature radius R_0 due to this, for increasing values of α, the marginally small surface of the disk is in contact with fluid particles and which provides less resistance between the particles and improves the liquid flow. Interestingly, a similar trend is recorded for increasing values of ε and this is because R_0 is a decreasing function of ε which enhances liquid flow and reduces the concentration distribution (See Figure 4(a) to 4(d)). Figure 5(a) and 5(b) elucidates the impact of β and Mn on $f(\xi)$ and $g(\xi)$. It is clear from these figures that increasing the value of β results in diminishing fluid velocity which resist the liquid flow. As Casson parameter approaches larger values, fluid starts to behave like a Newtonian fluid. Physically, an increase in β means $(\beta\rightarrow\infty)$, a decrease in the yield stress, hence reduction in boundary layer thickness is recorded. The applied magnetic field has the ability to slow down the momentum of fluid and this leads to decays in momentum boundary layer thickness. Therefore, increasing Mn reduces the radial and tangential velocity profiles. The impact of Re and n on the radial, tangential velocity and concentration fields are plotted in Figure 6. Both radial and tangential velocity increases as Re increases and it is because of the fact that larger $\mathrm{Re}=(\Omega R_0^2/\nu)$, results in viscous force decay, due to this momentum boundary layer thickness enhanced, whereas the reverse trend is observed in the case power law exponent parameter n (See Figure 6(a) and 6(b)). Figure 6(c) elucidates the impact of Re on $\phi(\xi)$. An Increment in Re results in the decrease of concentration profiles whereas the power-law exponent parameter increases the profiles. Influence of slip parameters γ_1 and γ_2 on velocity fields are plotted in Figure 7(a). As γ_1 and γ_2 increases, both radial and tangential velocities decays and results in the squeeze of the momentum boundary layer thickness and in the case of A1, the results are opposite to that of the slip parameters. Physically, an increase in the scaled stretching parameter produces more pressure on the fluid flow and hence enhancement in the radial velocity field is recorded (See Figure 7 (b)). Impact of the strength of the homogeneous reaction parameter K and strength of heterogeneous reaction parameter k_s on the concentration profile $\phi(\xi)$ is analyzed in Figure 8. In addition to this, the behaviour of Sc is also examined. Since the chemical reactants are consumed when the homogeneous reaction occurs, for larger values of K the concentration distribution $\phi(\xi)$ reduces (See Figure 8 (a)). Further, for higher values of k_s, raise in the concentration distribution $\phi(\xi)$ is observed. Rising behaviour of concentration profile is noted for higher values of Schmidt number Sc. The impact of physical parameters on $f'(0)$ and $g'(0)$ is presented in Table 3. It is noticed that an increase in Mn, n and β reduces the skin friction coefficient whereas the reverse trend is observed in the case of Reynolds number Re.

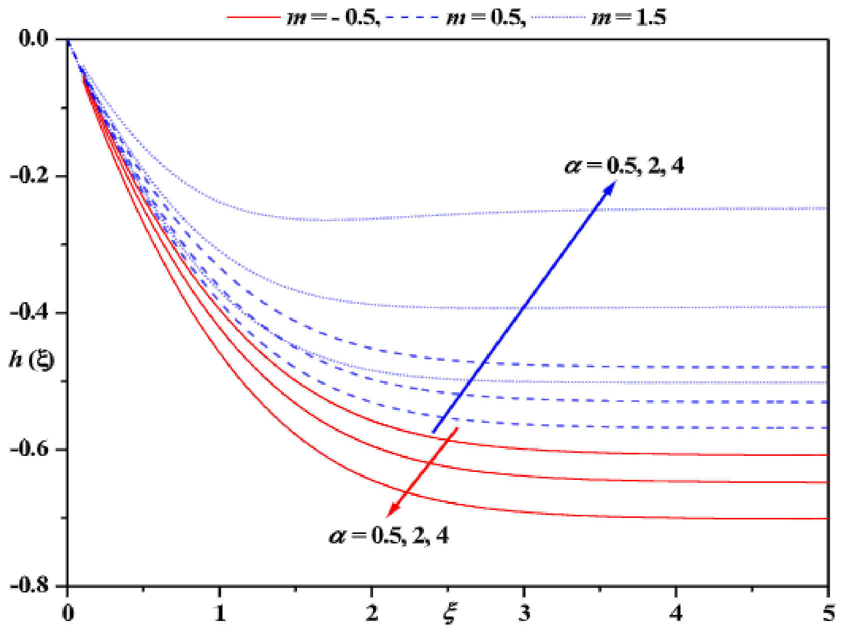

Fig. 3(a). Axial velocity profiles for different values of α and m, with Re = 1.5 , $A_1 = \varepsilon = \gamma_1$ =0.3, $Sc = k_s = n = K$ =0.5,β=2, γ_2 =0.4, Mn =1

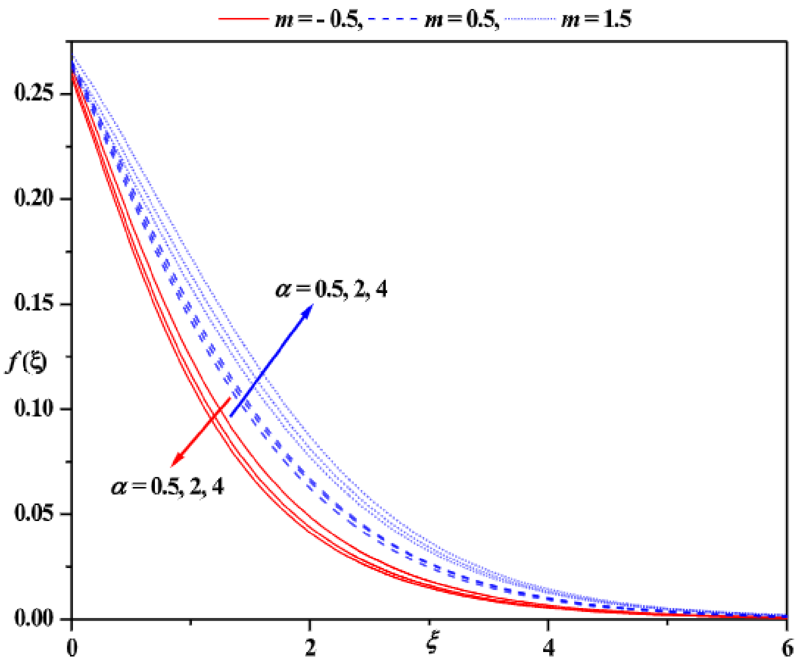

Fig. 3(b). Radial velocity profiles for different values of α and m, with Re = 1.5 , $A_1 = \varepsilon = \gamma_1$ =0.3, $Sc = k_s = n = K$ =0.5,β=2, γ_2 =0.4, Mn =1

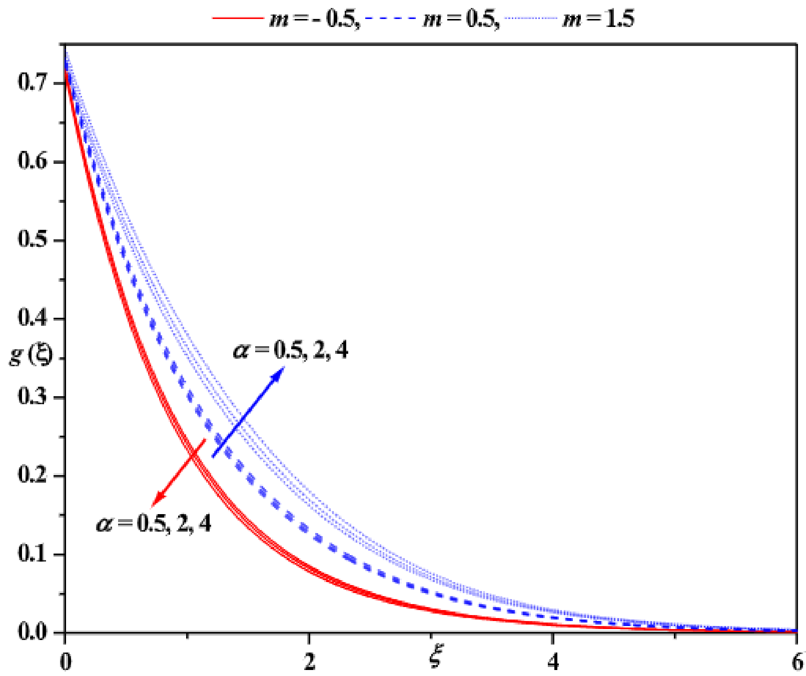

Fig. 3(c). Tangential velocity profiles for different values of α and m, with Re = 1.5 , A_1= ε = γ_1 =0.3, Sc = k_s =n= K =0.5,β=2, γ_2 =0.4, Mn =1

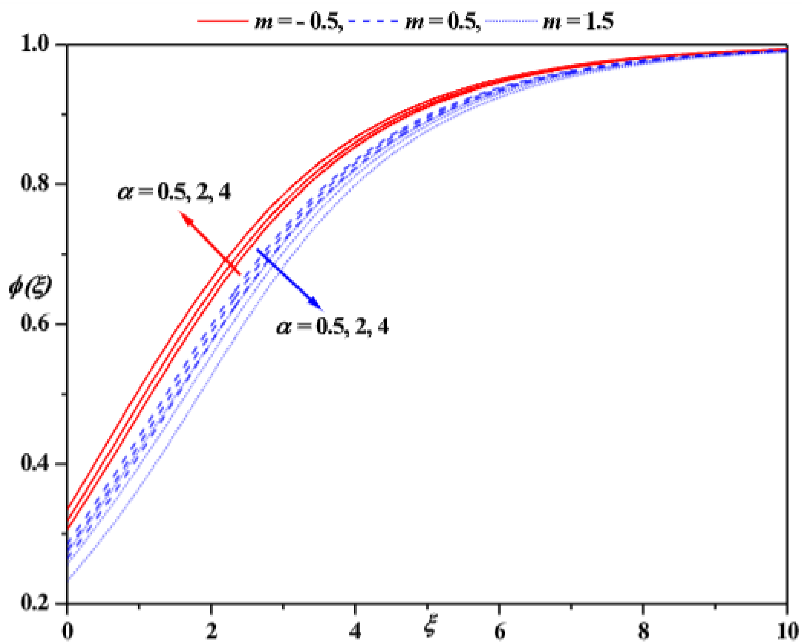

Fig. 3(d). Concentration profiles for different values of α and m, with Re = 1.5 , A_1= ε = γ_1 =0.3, Sc = k_s =n= K =0.5,β=2, γ_2 =0.4, Mn =1

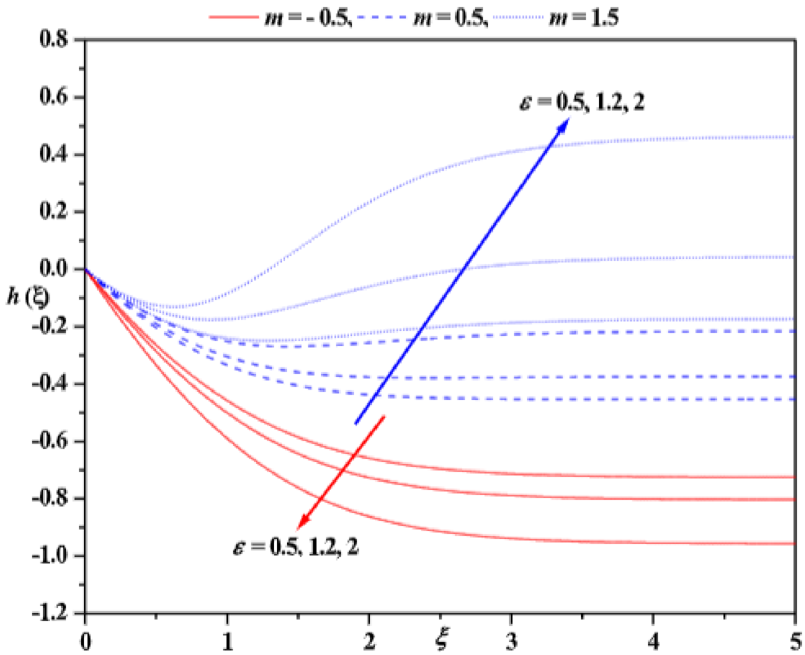

Fig. 4(a). Axial velocity profiles for different values of ε and m, with Re = 1.5 , $A_1=\gamma_1$=0.3, α=1.2, $Sc = k_s = n = K$ =0.5, β=2, γ_2=0.4, Mn =1

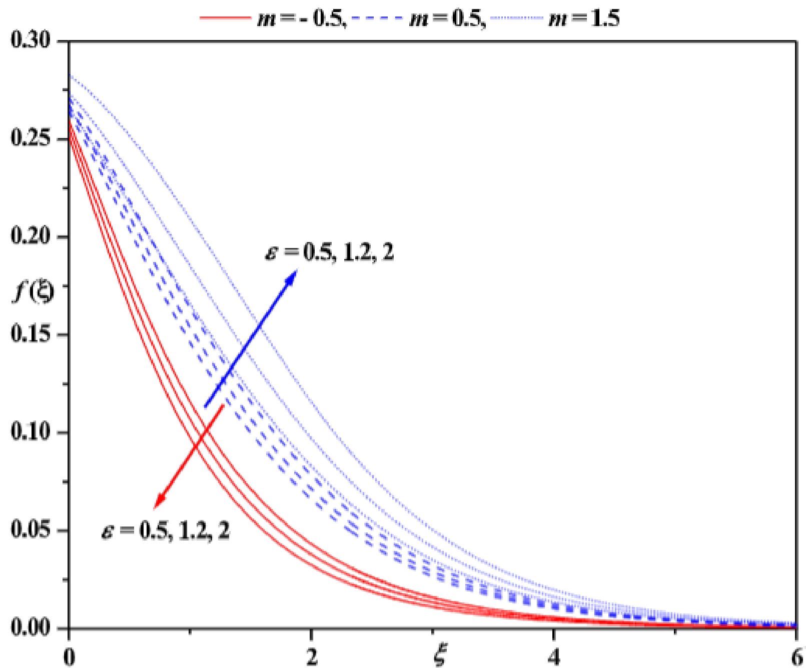

Fig. 4(b). Radial velocity profiles for different values of ε and m, with Re = 1.5 , $A_1=\gamma_1$=0.3, α=1.2, $Sc = k_s = n = K$ =0.5, β=2, γ_2=0.4, Mn =1

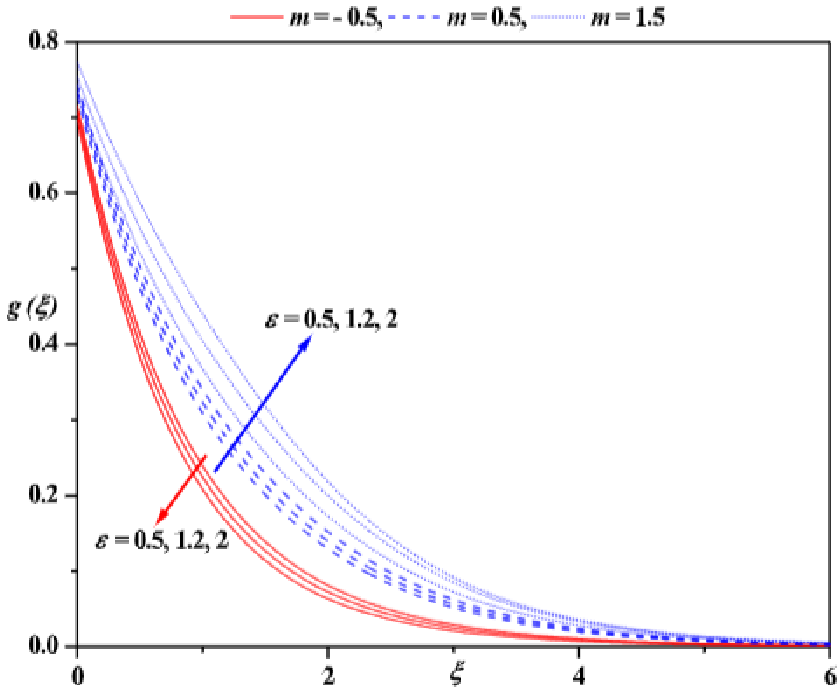

Fig. 4(c). Tangential velocity profiles for different values of ε and m, with Re = 1.5 , A_1=γ_1=0.3, α=1.2, Sc = k_s =n= K =0.5,β=2, γ_2 =0.4, Mn =1

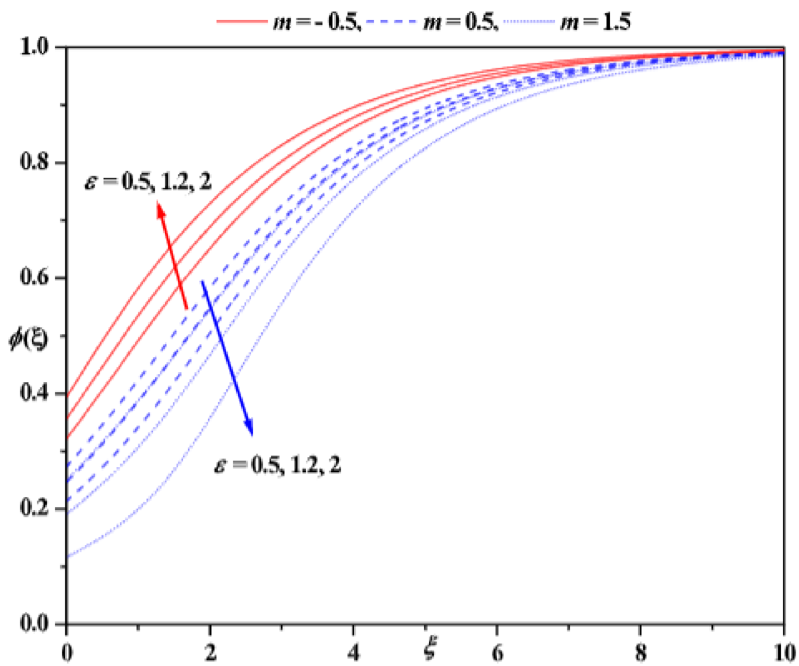

Fig. 4(d). Concentration profiles for different values of ε and m, with Re = 1.5 , A_1=γ_1=0.3, α=1.2, Sc = k_s =n= K =0.5,β=2, γ_2=0.4, Mn =1

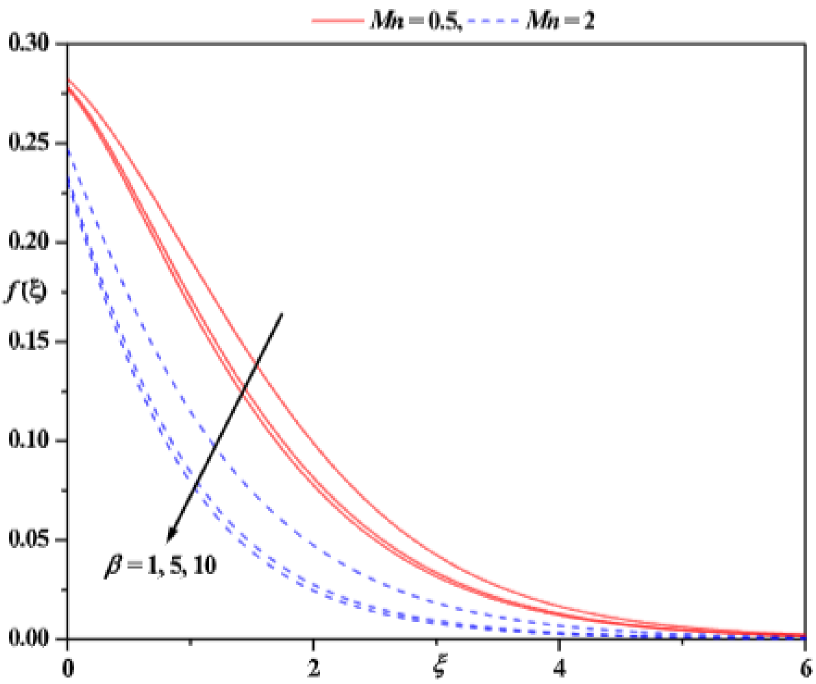

Fig. 5(a). Radial velocity profiles for different values of β and Mn with Re = 1.5 , $A_1 = \varepsilon = \gamma_1$ =0.3, α=1.2, $Sc = m, = k_s = n = K$ =0.5, γ_2 =0.4

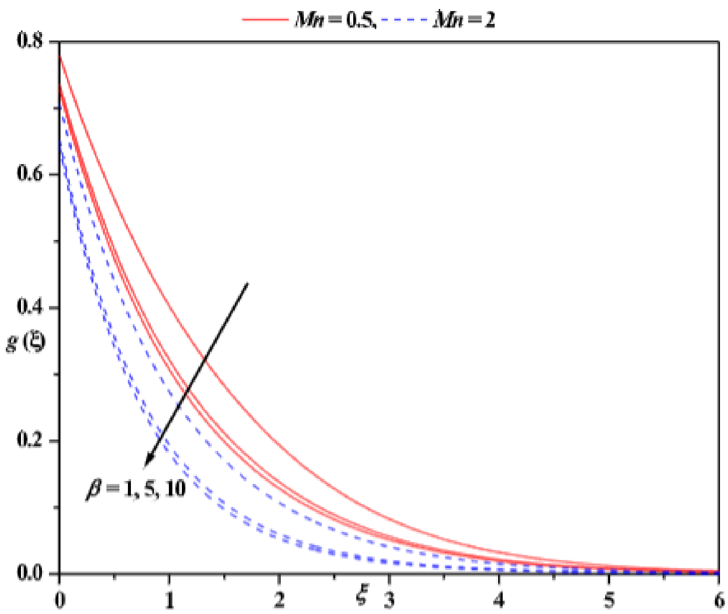

Fig. 5(b). Tangential velocity profiles for different values of β and Mn with Re = 1.5 , $A_1 = \varepsilon = \gamma_1$ =0.3, α=1.2, $Sc = m, = k_s = n = K$ =0.5, γ_2 =0.4

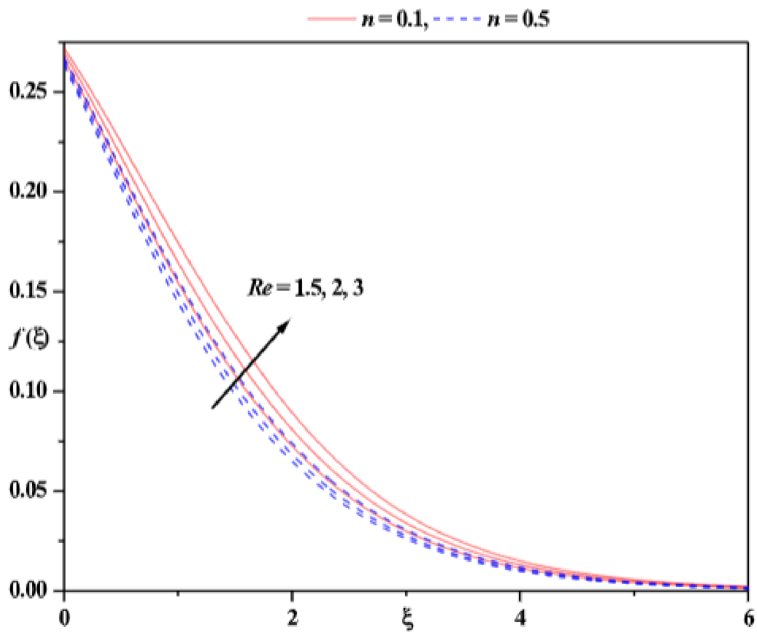

Fig. 6(a). Radial velocity profiles for different values of Re and *n* with Mn =1, A_1= ε = γ_1 =0.3, α=1.2, Sc = m, = k_s = K =0.5, β=2, γ_2 =0.4

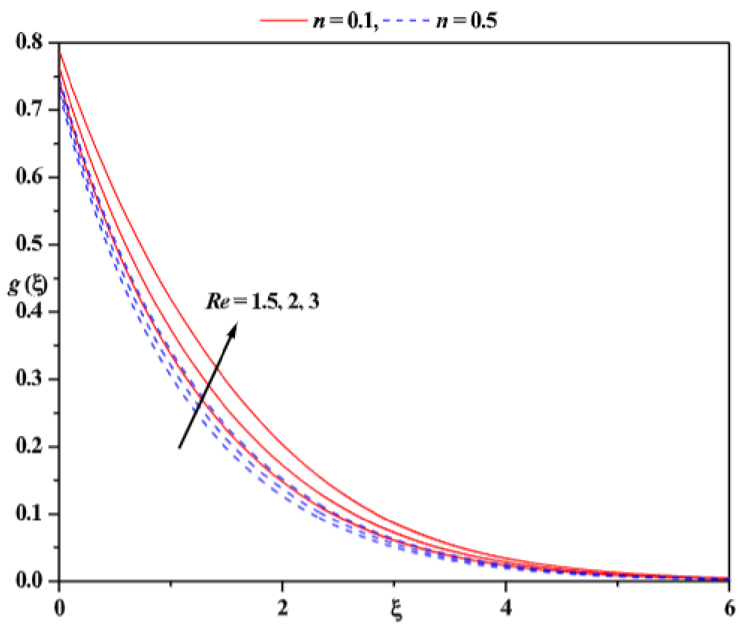

Fig. 6(b). Tangential velocity profiles for different values of Re and *n* with Mn =1, A_1= ε = γ_1 =0.3, α=1.2, Sc = m, = k_s = K =0.5, β=2, γ_2 =0.4

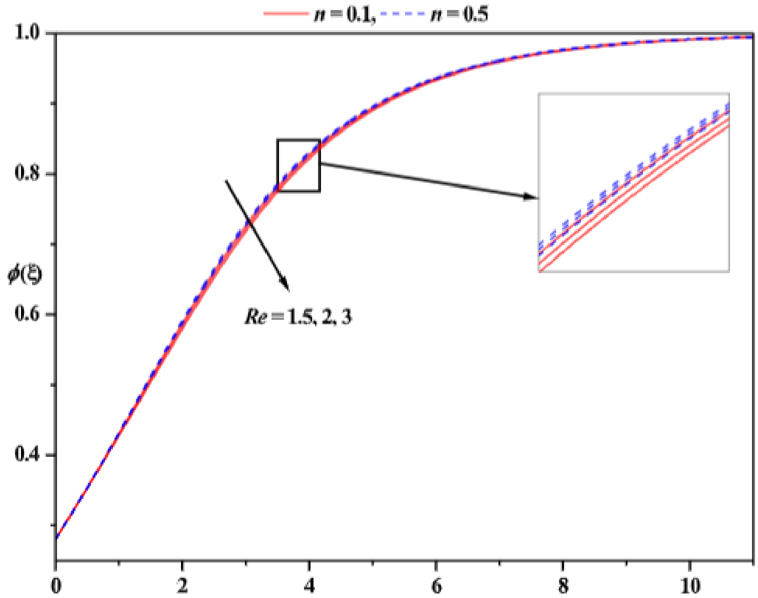

Fig. 6(c). Concentration profiles for different values of Re and *n* with Mn =1, A_1= ε = γ_1 =0.3, α=1.2, Sc = m, = k_s = K =0.5, β=2, γ_2 =0.4

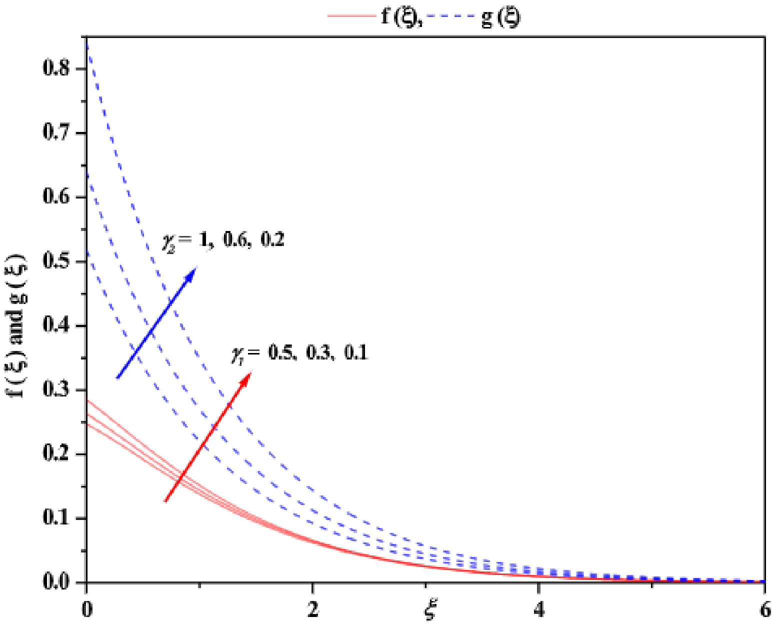

Fig. 7(a). Radial and Tangential velocity profiles for different values of γ_1 and γ_2 with Re=1.5, A_1= ε =0.3, α=1.2, n= Sc = m, = k_s = K =0.5, β=2, Mn =1

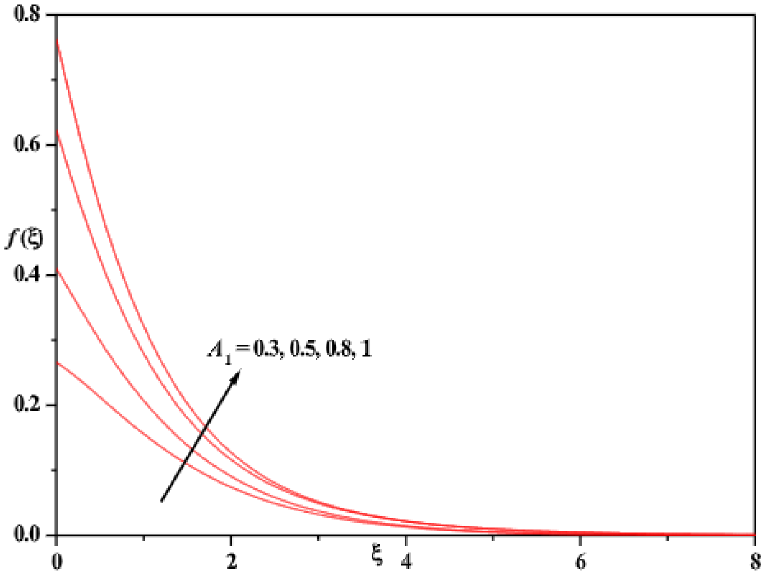

Fig. 7(b). Radial velocity profiles for different values of A_1 with Re=1.5, Mn =1, ε = γ_1=0.3, Sc = m, =k_s = K =n=0.5, β=2, γ_2 =0.4, α=1.2

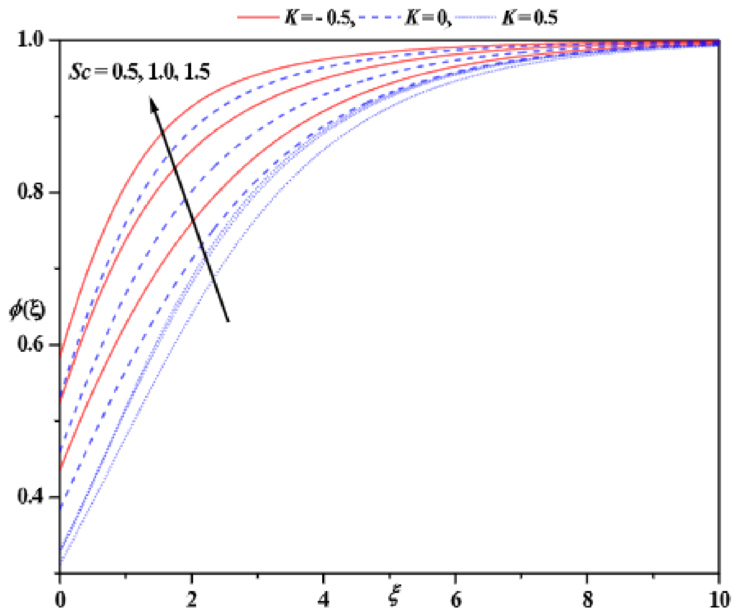

Fig. 8(a). Concentration profiles for different values of Sc and K with Re=1.5, A_1 = ε = γ_1 =0.3, α=1.2, n = m, =k_s = 0.5, β=2, Mn =1, γ_2 =0.4

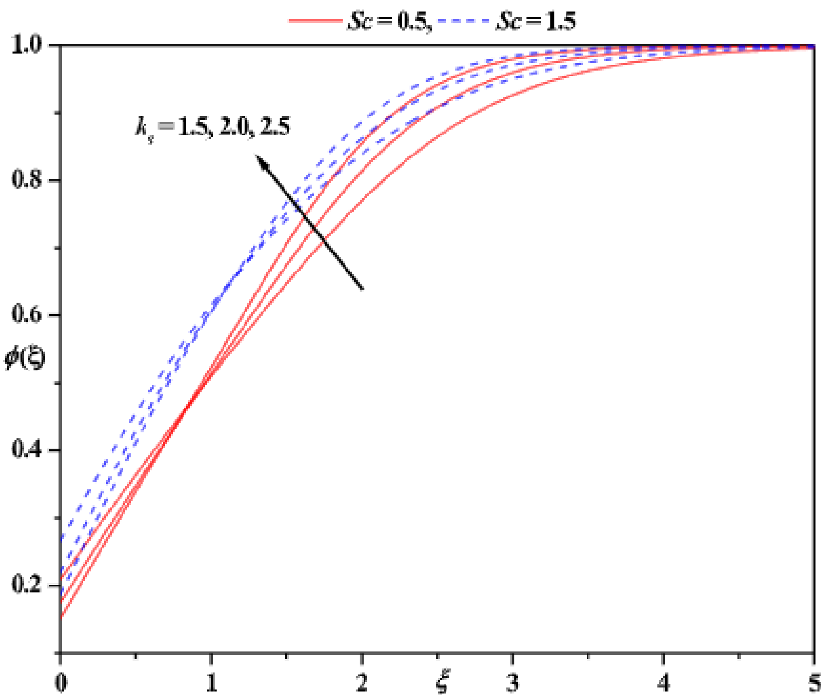

Fig. 8(b). Concentration profiles for different values of Sc and k_s with Re=1.5, $A_1 = \varepsilon = \gamma_1$ =0.3, α=1.2, $n = m, = K$ = 0.5, β=2, Mn =1, γ_2 =0.4

Table 3
Values of skin friction, convergence control parameter and average squared residual error for different physical parameters with $A_1 = 0.3, k_s = Sc = K = 0.5$

γ_1	γ_2	Re	n	Mn	β	m	ε	α	$-f'(0)$	$-\hbar_f$	$\bar{E}_{10}^{f}$	$-g'(0)$	$-\hbar_g$	$\bar{E}_{10}^{g}$	CPU Time(sec)
								0.5	0.13535	0.34962	$1.50\text{x}10^{-7}$	0.76623	1.07266	$4.24\text{x}10^{-7}$	523.49
						-0.5		2	0.14627	1.04145	$6.69\text{x}10^{-7}$	0.77603	1.08028	$5.11\text{x}10^{-7}$	515.18
0.3	0.5	1.5	0.5	1	2		0.3	4	0.15353	1.04764	$8.07\text{ x}10^{-7}$	0.78907	1.08985	$6.51\text{ x}10^{-7}$	563.64
								0.5	0.11281	0.52162	$3.66\text{ x}10^{-7}$	0.62934	0.74742	$3.35\text{ x}10^{-7}$	504.16
						0.5		2	0.10911	0.70818	$2.83\text{ x}10^{-7}$	0.62256	0.74554	$3.31\text{ x}10^{-6}$	533.01
								4	0.10447	0.60482	$1.41\text{ x}10^{-7}$	0.61353	0.74379	$3.37\text{ x}10^{-6}$	530.68
							0.5		0.14732	1.04254	$7.11\text{ x}10^{-7}$	0.77751	1.08152	$5.43\text{ x}10^{-7}$	561.82
						-0.5	1.2		0.16011	1.05418	$1.04\text{ x}10^{-6}$	0.80074	1.09835	$9.08\text{ x}10^{-7}$	577.87
0.3	0.5	1.5	0.5	1	2		2	1.2	0.17627	1.06472	$1.38\text{ x}10^{-6}$	0.82677	1.11048	$1.49\text{ x}10^{-6}$	550.61
							0.5		0.10831	0.70388	$2.12\text{ x}10^{-7}$	0.62135	0.74526	$3.22\text{ x}10^{-6}$	538.81
						0.5	1.2		0.09875	0.68892	$1.54\text{ x}10^{-8}$	0.60435	0.74314	$3.39\text{ x}10^{-6}$	502.08
							2		0.08757	0.71018	$1.29\text{ x}10^{-7}$	0.58472	0.74552	$5.16\text{ x}10^{-6}$	567.42
					1				0.05352	0.58382	$3.04\text{ x}10^{-5}$	0.50176	0.55623	$1.61\text{ x}10^{-5}$	528.33
				0.5	5				0.06445	0.89318	$2.61\text{ x}10^{-7}$	0.60112	0.93482	$3.71\text{ x}10^{-6}$	532.78
0.3	0.5	1.5	0.5		10	0.5	0.3	1.2	0.06791	0.99012	$4.51\text{ x}10^{-7}$	0.64966	1.01311	$2.08\text{ x}10^{-6}$	535.46
					1				0.09772	0.55368	$2.01\text{ x}10^{-6}$	0.56621	0.55775	$9.62\text{ x}10^{-6}$	500.25
				1	5				0.12436	0.90232	$4.75\text{ x}10^{-7}$	0.67584	0.92467	$7.61\text{ x}10^{-7}$	511.62
					10				0.13014	0.97888	$3.59\text{ x}10^{-7}$	0.69578	1.00429	$3.79\text{ x}10^{-7}$	497.99
		1.5							0.10112	0.59072	$3.65\text{ x}10^{-7}$	0.58989	0.61326	$7.71\text{ x}10^{-6}$	528.57
		2	0.1						0.09231	0.49288	$1.11\text{ x}10^{-5}$	0.53782	0.47568	$9.84\text{ x}10^{-6}$	530.46
0.3	0.5	3		1	2	0.5	0.3	1.2	0.08456	0.36592	$1.06\text{ x}10^{-4}$	0.48151	0.33624	$3.72\text{ x}10^{-6}$	531.54
		1.5							0.11058	0.71098	$3.27\text{ x}10^{-7}$	0.62537	0.74625	$3.31\text{ x}10^{-6}$	522.19
		2	0.5						0.10581	0.60152	$1.99\text{ x}10^{-8}$	0.60485	0.67888	$5.31\text{ x}10^{-6}$	531.62
		3							0.09965	0.57746	$8.06\text{ x}10^{-7}$	0.57687	0.59172	$8.48\text{ x}10^{-6}$	539.34
	0.2								0.08601	0.50817	$6.87\text{x}10^{-7}$	0.62257	0.74485	$5.97\text{x}10^{-6}$	532.74
0.3	0.6	1.5	0.5	1	2	0.5	0.3	1.2	0.12781	0.70677	$1.48\text{x}10^{-7}$	0.54829	0.74692	$2.05\text{x}10^{-6}$	540.29
	1.0								0.14837	0.59622	$2.94\text{x}10^{-8}$	0.44015	0.74625	$9.51\text{x}10^{-7}$	539.89
0.1									0.13241	0.52218	$2.35\text{x}10^{-7}$	0.63176	0.75121	$3.15\text{x}10^{-6}$	563.68
0.3	0.4	1.5	0.5	1	2	0.5	0.3	1.2	0.11103	0.71219	$3.53\text{x}10^{-7}$	0.62618	0.74651	$6.57\text{x}10^{-6}$	554.09
0.5									0.09575	0.71852	$3.51\text{x}10^{-7}$	0.62207	0.74491	$6.52\text{x}10^{-6}$	570.86

4. Conclusions

In the present paper, we examined the impact of homogeneous and heterogeneous reaction on Casson fluid due to a stretchable rotating disk in the presence of slip effects and variable thickness. Some of the interesting points as follows,

I. Fluid concentration increases due to raising the values of the Schmidt number and power-law exponent parameter.
II. The opposite trend is observed in the case of homogeneous reaction parameter and heterogeneous reaction parameter.
III. Increasing values of Slip parameter, Casson parameter and Hartmann number oppose the fluid flow.
IV. For increasing the values of disk thickness coefficient and dimensionless constant, momentum boundary layer thickness enhanced whereas the reverse trend is recorded in the case of concentration distribution.

Acknowledgments
The authors appreciate the constructive comments of the reviewers which led to definite improvement in the paper.

References

[1] Karman,T.V. "UberLaminare and TurbulenteReibung." *ZeitschriftfürAngewandteMathematik undMechanik* 1, no. 4 (1921): 232-252.
[2] Cochran, W. G. "The flow due to a rotating disc." *In Mathematical Proceedings of the Cambridge Philosophical Society,* vol. 30, no. 3, pp. 365-375. Cambridge University Press, 1934.
[3] Batchelor, Go K. "Note on a class of solutions of the Navier-Stokes equations representing steady rotationally-symmetric flow." *The quarterly journal of mechanics and applied mathematics* 4, no. 1 (1951): 29-41.
[4] Stewartson, K. "On the flow between two rotating coaxial disks." In *Mathematical Proceedings of the Cambridge Philosophical Society*, vol. 49, no. 2, pp. 333-341. Cambridge University Press, 1953.
[5] Benton, Edward R. "On the flow due to a rotating disk." *Journal of Fluid Mechanics* 24, no. 4 (1966): 781-800.
[6] Andersson, H. I., E. De Korte, and R. Meland. "Flow of a power-law fluid over a rotating disk revisited." *Fluid dynamics research* 28, no. 2 (2001): 75-88.
[7] Ming, Chunying, Liancun Zheng, and Xinxin Zhang. "Steady flow and heat transfer of the power-law fluid over a rotating disk." *International Communications in Heat and Mass Transfer* 38, no. 3 (2011): 280-284.
[8] Khidir, Ahmed A. "Viscous dissipation, Ohmic heating and radiation effects on MHD flow past a rotating disk embedded in a porous medium with variable properties." *Arabian Journal of Mathematics* 2, no. 3 (2013): 263-277.
[9] Chenguang Yin, LiancunZheng, Chaoli Zhang, and XinxinZhang."Flow and Heat Transfer of nanofluids over a Rotating Porous Disk with Velocity Slip and Temperature Jump." *Z. Naturforsch* 70, no. 5 (2015): 351–358.
[10] Sheikholeslami, M., M. Hatami, and D. D. Ganji. "Numerical investigation of nanofluid spraying on an inclined rotating disk for cooling process." *Journal of Molecular Liquids* 211 (2015): 577-583.
[11] Yin, Chenguang, Liancun Zheng, Chaoli Zhang, and Xinxin Zhang. "Flow and heat transfer of nanofluids over a rotating disk with uniform stretching rate in the radial direction." *Propulsion and Power Research* 6, no. 1 (2017): 25-30.
[12] Fang, T., Zhang, J. and Zhong, Y. "Boundary layer flow over a stretching sheet with variable thickness." *Applied Mathematics &computation* 218 (2012): 7241–7252.
[13] Xun, Shuo, Jinhu Zhao, Liancun Zheng, Xuehui Chen, and Xinxin Zhang. "Flow and heat transfer of Ostwald-de Waele fluid over a variable thickness rotating disk with index decreasing." *International Journal of Heat and Mass Transfer* 103 (2016): 1214-1224.

[14] Hayat, Tasawar, Sumaira Qayyum, Maria Imtiaz, and Ahmed Alsaedi. "Radiative flow due to stretchable rotating disk with variable thickness." *Results in Physics* 7 (2017): 156-165.

[15] Imtiaz, Maria, Tasawar Hayat, Ahmed Alsaedi, and Saleem Asghar. "Slip flow by a variable thickness rotating disk subject to magnetohydrodynamics." *Results in Physics* 7 (2017): 503-509.

[16] Prasad, K. V., K. Vajravelu, I. S. Shivakumara, Hanumesh Vaidya, and Neelufer Basha. "Flow and heat transfer of a Casson Nanofluid over a nonlinear stretching sheet." *Journal of Nanofluids* 5, no. 5 (2016): 743-752.

[17] Prasad, K. V., K. Vajravelu, and Hanumesh Vaidya. "MHD Casson nanofluid flow and heat transfer at a stretching sheet with variable thickness." *Journal of Nanofluids* 5, no. 3 (2016): 423-435.

[18] Prasad, K. V., K. Vajravelu, Hanumesh Vaidya, and Robert A. Van Gorder. "MHD flow and heat transfer in a nanofluid over a slender elastic sheet with variable thickness." *Results in physics* 7 (2017): 1462-1474.

[19] Prasad, K. V., Hanumesh Vaidya, K. Vajravelu, and V. Ramanjini. "Analytical study of Cattaneo-Christov heat flux model for Williamson-nanofluid flow over a slender elastic sheet with variable thickness." *Journal of Nanofluids* 7, no. 3 (2018): 583-594.

[20] Prasad, K.V., Hanumesh Vaidya, Makinde, O.D., SrikanthaSetty, B., "MHD mixed convective flow of Cassonnanofluid over a slender rotating disk with source/sink and partial slip effects." *Defect and Diffusion Forum* 392 (2019): 92-122.

[21] Chaudhary, M. A., and J. H. Merkin. "A simple isothermal model for homogeneous-heterogeneous reactions in boundary-layer flow. I Equal diffusivities." *Fluid dynamics research* 16, no. 6 (1995): 311.

[22] Chaudhary, M.A. and Merkin, J.H. "A simple isothermal model for Homogeneous- Heterogeneous reactions in boundary layer flow: II different for diffusivities reactant and autocatalyst." *Fluid dynamics research* 16 (1995): 335-359.

[23] Merkin, J. H. "A model for isothermal homogeneous-heterogeneous reactions in boundary-layer flow." *Mathematical and Computer Modelling* 24, no. 8 (1996): 125-136.

[24] Bachok, Norfifah, Anuar Ishak, and Ioan Pop. "On the stagnation-point flow towards a stretching sheet with homogeneous–heterogeneous reactions effects." Communications in Nonlinear Science and Numerical Simulation 16, no. 11 (2011): 4296-4302.

[25] Kameswaran, P. K., S. Shaw, P. Sibanda, and P. V. S. N. Murthy. "Homogeneous–heterogeneous reactions in a nanofluid flow due to a porous stretching sheet." *International journal of heat and mass transfer* 57, no. 2 (2013): 465-472.

[26] Hayat, Tasawar, Muhammad Ijaz Khan, Ahmad Alsaedi, and Muhammad Imran Khan. "Homogeneous-heterogeneous reactions and melting heat transfer effects in the MHD flow by a stretching surface with variable thickness." *Journal of Molecular Liquids* 223 (2016): 960-968.

[27] Hayat, Tasawar, Maria Imtiaz, Ahmed Alsaedi, and Faris Alzahrani. "Effects of homogeneous–heterogeneous reactions in flow of magnetite-Fe3O4 nanoparticles by a rotating disk." *Journal of Molecular Liquids* 216 (2016): 845-855.

[28] Lavanya, Bommanna. "MHD Rotating Flow Through a Porous Medium with Heat and Mass Transfer." *Journal of Advanced Research in Fluid Mechanics and Thermal Sciences* 54, no. 2 (2019): 221-231.

[29] Tourab, M., and Aguib, S., "Experimental Analysis of the Thermal effect of the magneto mechanical behaviour of viscoelastic elastomer." *Journal of Advanced Research in Fluid Mechanics and Thermal Sciences* 53, no. 1 (2019): 25-34.

[30] Bhat, Ashwini, and Nagaraj N. Katagi. "Analysis of Stagnation Point flow of an Incompressible Viscous Fluid between Porous Plates with Velocity Slip." *Journal of Advanced Research in Fluid Mechanics and Thermal Sciences* 48, no. 1 (2018): 40-52.

[31] Choudhari, Rajashekhar, Manjunatha Gudekote, and Naveen Choudhari. "Analytical Solutions on the Flow of blood with the Effects of Hematocrit, Slip and TPMA in a porous tube." *Journal of Advanced Research in Fluid Mechanics and Thermal Sciences* 47, no. 1 (2018): 201-208.

[32] Wakif, Abderrahim, Zoubair Boulahia, and Rachid Sehaqui. "A semi-analytical analysis of electro-thermo-hydrodynamic stability in dielectric nanofluids using Buongiorno's mathematical model together with more realistic boundary conditions." *Results in Physics* 9 (2018): 1438-1454.

[33] Wakif, Abderrahim, Zoubair Boulahia, Farhad Ali, Mohamed R. Eid, and Rachid Sehaqui. "Numerical analysis of the unsteady natural convection MHD couette nanofluid flow in the presence of thermal radiation using single and Two-Phase nanofluid models for Cu–Water nanofluids." *International Journal of Applied and Computational Mathematics* 4, no. 3 (2018): 81.

[34] Wakif, Abderrahim, Zoubair Boulahia, S. R. Mishra, Mohammad Mehdi Rashidi, and Rachid Sehaqui. "Influence of a uniform transverse magnetic field on the thermo-hydrodynamic stability in water-based

nanofluids with metallic nanoparticles using the generalized Buongiorno's mathematical model." *The European Physical Journal Plus* 133, no. 5 (2018): 181.

[35] Ali, H.M., Ali, H., Abubaker, M., Saieed, A., William P.A.O., Majid, A., Hasan, K., "Condensate retention as a function of condensate flow rate on 1 horizontal enhanced pin-fin tubes." *Thermal Science*, no. 103 (2018): 161-161.

[36] Rabihah, M.S., "Using mathematics to quantify subjective decisions: applications of analytic hierarchy process to risk assessment." *Journal of Advanced Research Design* 44, no. 1 (2018): 7-19.

[37] Liao, Shijun. "An optimal homotopy-analysis approach for strongly nonlinear differential equations." *Communications in Nonlinear Science and Numerical Simulation* 15, no. 8 (2010): 2003-2016.

[38] Van Gorder, Robert A. "Optimal homotopy analysis and control of error for implicitly defined fully nonlinear differential equations." *Numerical Algorithms* (2018): 1-16.